Manuskripteingang: 12. 5. 1983

AKADEMIE DER WISSENSCHAFTEN DER DDR
ZENTRALINSTITUT FÜR ELEKTRONENPHYSIK
1086 Berlin, Mohrenstraße 40/41

Ag 521/606/83

ZIE

Akademie der Wissenschaften der DDR
Zentralinstitut für Elektronenphysik

Preprint 83-3

# INVESTIGATIONS OF THE START UP PHASE IN THE TM 1 TOKAMAK

H. Prinzler, P. Heymann, H. Stoeckl, H. Badalec
F. Zacek, K. Jakubka, V. Kopecky

Mai 1983

# INVESTIGATIONS OF THE START UP PHASE IN THE TM 1 TOKAMAK

H. Prinzler, P. Heymann
Zentralinstitut für Elektronenphysik
der AdW der DDR
1199 Berlin DDR

H. Stoeckl, H. Badalec, F. Zácek, K. Jakubka,
V. Kopecký
Institute of Plasma Physics CSAV
180 69 Prague 8 CSSR

März 1983

Investigation of the Start up phase in the

TM 1 Tokamak

## 1. INTRODUCTION

The start up phase of a Tokamak discharge has been investigated by several authors during the last decade.
In the papers of DIMOCK et al. /1/, HUTCHINSON and STRACHAN /2/, STRACHAN /3/ and PAPOULAR /4/ the intention was mainly a general understanding of the processes of breakdown in toroidal geometry and their time scale. The optimization of the start up i.e. the minimum energy demand for the plasma formation was the aim of the investigations of ABRAMOV et al. /5//6/ and SOMETANI and FUJISAWA /7/. The problem of intense plasma wall interaction in this time range is the subject of two papers by STRACHAN /8/ and DENISOV et al. /9/.

Apart from some details the following qualitative picture is accepted. The discharge runs through different states until reaching the stationary hot plasma. The first one is the gas breakdown with exponential current growth (avalanche phase). Above a certain plasma current ($I_p$ = 1kA for TM 1) the rotational transform establishes and the plasma confinement begins with a pinch phase. The electron density is still increasing until the plasma is fully ionized. In this time period gas discharge processes as excitation, ionization and H-atom radiation take place, therefore the bulk electron temperature remains low ($T_e$< 20 eV). Plasma heating starts but now when the plasma has been fully ionized.

One of the open questions is, to our opinion, the long time delay between ignition of the OH-battery and the appearance of the first microwave signal, say n = $10^{12}$ $cm^{-3}$. DENISOV et al. /9/ explained the time lag of the T 7 start up by the ion time of flight being much longer than the time constant of the avalanche growth. We did not confirm this model in the present experiments where we investigated especially the avalanche phase of the plasma evolution in the TM 1 Tokamak.

The paper is organized as follows: The experiments are described in Sec. 2. There we report on basic parameters

(2.1), plasma position (2.2) and probe measurements (2.3). In Sec. 3 we give a quantitative model of the avalanche phase. First we deal with the electrodynamical properties i.e. the evaluation of plasma field and current (3.1) and the determination of plasma resistance and electron density (3.2). The time constant of the electron density evolution is discussed in (3.3). The comparison of our model with experimental results is given in Sec. 4. We discuss the influence of transverse magnetic fields and the ionization rate under our conditions. Conclusions are given in Sec. 5.

## 2. EXPERIMENTAL ARRANGEMENTS AND RESULTS

### 2.1 Basic parameters

The Tokamak TM 1 has been described earlier /10/. We made the following experiments with a toroidal magnetic field $B_T$ = 1,3 T, a maximum plasma current $I_p$ = 16 kA and a variation of the vertical and horizontal magnetic fields generated by the separate coil systems: $B_V = \pm 2{,}25 \cdot 10^{-3}$ T ($2{,}8 \cdot 10^{-3}$ T/kA) and $B_H$ 0...$3{,}25 \cdot 10^{-3}$ T ($6{,}5 \cdot 10^{-3}$ T/kA). The filling pressure is $p = 1{,}2 \cdot 10^{-2}$ Pa without additional gas puffing that means $n_H = 7 \cdot 10^{12}$ H-atoms/cm$^3$ after dissociation. Diagnostic methods and the direction of fields and current are shown in Fig. 1. In the limiter shadow there are two Langmuir probes (Mo-wire l = 5mm, d = 1 mm) which can be shifted from the liner position to the very edge of the limiter projection. The $H_\beta$-line radiance is measured through the collimator of the neutral beam diagnostics at different positions $\Delta$h. The receiving system is a photomultiplier with interference filter. Relative values are obtained only. We did not succeed in measuring the carbon C III and C V lines with a similar filter in the $\lambda$ = 230 mm range since it did not reject the H-radiation sufficiently. The bright H-radiation during the start up phase covers the weak C-radiation within the first 500 /us.



We made a series of shots with variing $B_v$ and $B_h$ in order to reveal their influence on the current rise and the temporal evolution of the other plasma parameters.

The temporal evolution of a typical discharge is shown in Fig. 2. The data of loop voltage $U_l$, total current $I_t$ (liner + plasma current), mean electron density n (from 4 mm /u-wave interferometer) and ion saturation current $I_+$ of the probe in the limiter shadow can be measured directly. The plasma current $I_p$ is obtained from the total current and the loop voltage $U_l$:

$$I_p = I_t - I_{Liner} = I_t - \frac{U_l}{Z_l}$$

The ohmic liner resistance $Z_l$ has been determined from shots without plasma and also from the first 100 /us of a plasma discharge to $Z_l$ = 40 m$\Omega$ . The inductive part of the liner current can be neglected ($L_l \leq$ 40 nH).

The Langmuir probe signal showing the density of the scrape-off layer (SOL) plasma can be used to denote the different regimes of the plasma formation. The first phase lasting up to t = 150-200 /us is the breakdown in the whole cross section of the liner, we call it avalanche phase. In the following time period from t = 200-350 /us the plasma disappears from the limiter shadow due to the beginning confinement by the plasma current poloidal magnetic field, we call it pinch phase. After that the probe signal indicates again the presence of plasma which moves from the centre into the limiter shadow forming there the SOL-plasma of the stationary state.

Three typical current rises in dependence on the external $B_v$ and $B_h$ fields are shown in Fig. 3. The avalanche phase is characterized by an exponential growth $\exp(\gamma t)$ the time constant of which $1/\gamma$ depends on the perpendicular fields. The next period with the slower increase is the pinch phase starting above $I_p$ = 1 kA.

## 2.2 Position of the plasma column

A strong change of the radial profile of the plasma column takes place during the process of breakdown and the evolution of the Tokamak plasma. The avalanche phase is characterized by a homogeneous distribution with a flat profile. The both probes (upper and lower) show nearly equal values of ion saturation current (Fig. 4a). The radial profile of the $H_\beta$-radiation is also flat in that time interval. No part of the cross section shows enhanced radiance (Fig.4b). A distinct change starts with the end of the avalanche phase at t = 200/us. The plasma pinches and the centre of the column moves from the bottom to the top with a velocity of $v = 2 \cdot 10^4$ cm/s.

All three diagnostic methods show that effect: Mirnovcoil signal of the plasma current position, maximum and radial front of the $H_\beta$-radiance and the ion saturation current of the probe (Fig. 4c). The upper probe is reached 300/us after ignition of the OH-battery. The time when the plasma front reaches the probe at different positions gives also the velocity $v = 2 \cdot 10^4$ cm/s.

The position of the current maximum does not coincide with the $H_\beta$ maximum but shows also the upward directed motion with the same velocity.

The high position of the plasma column in the stationary state is striking. The difference in density measured by the upper and lower probe is two orders of magnitude. That plasma position is present in every normal shot and cannot be influenced by the external perpendicular fields. An increase of $B_h$ to press the plasma down leads only to disruptive instabilities.

### 2.3 Probe measurements

The results of probe measurements in the SOL-plasma are shown in Fig. 5. Besides the routine observation of the ion saturation current we made a series of probe current measurements



in subsequent shots with a certain bias voltage for every shot. From these data we composed the Langmuir probe characteristics of Fig. 5a. There are fast electrons in the avalanche phase (up to 180/us) and a bulk electron temperature of 7-10 eV during the first 300/us (Fig. 5b). The floating potential decreases from $U_{fl}$ = 70-80 V to 5 V during the pinch phase (Fig. 5c). The density of the wall plasma decreases simultaneously (Fig. 5d). No fast electrons are present in that time period.

## 3. MODEL OF THE AVALANCHE PHASE

The theoretical description includes the simultaneous solution of many nonlinear processes as energy- and particle balance, Maxwell's equations, the equations for heat transfer and radiation losses as well as equations for the external electrical circuit. This is a tedious task which can be solved only numerically. To our knowledge the paper of ABRAMOV et al /6/ is the most comprehensive one which accounts for most of this processes. An additional difficulty arises if high energy electrons (run aways) must be taken into account.

The aim of the present model is much more restricted: it should be a guide to interprete the experimental facts and to give an explanation of some physical processes on the base of the experiments. The main striking facts are the fast current rise before pinching, and the dependence of the rise time on the auxiliary perpendicular magnetic fields. Consequently the model is limited to this phenomena.

### 3.1 The evolution of plasma field and current

The temporal evolution of the toroidal electric field inside the plasma and the current rise are discussed in the following part. We restrict ourselves to the avalanche phase where ionization is determined by the electric field $E_T$ impressed to the torus by the OH-battery. This phase is finished when the plasma is fully ionized and its conductivity corresponds to a temperature of 5 to 10 eV.

For simplicity we neglect the toroidal geometry and use a cylindrical model with a homogeneous conductivity. From probe measurements and observations of the optical radiation in the early state which show nearly flat profiles this assumption seemes to be justified. If a sufficient strong electric field $E_T = \frac{U_{loop}}{2\pi R_T}$ is impressed to the initial low density plasma+) ($n \simeq 10^7 \ldots 10^8 cm^{-3}$) we must account at least for the following processes:

a) ionization due to the electric field, controlled by the Townsend coefficient $\alpha(E)$, and the different carrier loss mechanisms;

b) temporal variation of the plasma conductivity $\sigma(t)$;

c) prevention of field penetration caused by the fast change of the conductivity (skin effect);

d) the relaxation process when the poloidal magnetic field is build up. It is the transient process of a L/R circuit with a nonlinear resistor $\propto 1/\sigma(t)$.

The problem is further simplified if the influence of the temporal varying electric field on $\sigma$ during the avalanche state can be neglected. In this case $\sigma(t)$ can be treated as a purely time depending parametric quantity. In part 3.2 and 3.3 it is shown, that the effective growth rate of the density ($\nu^i - \beta$) varies proportional to $\sqrt{E}$. For a moderate change of E during the avalanche state a constant mean growth rate can be assumed.

With this restrictions the equations of field diffusion (or skin effect)

$$\frac{\partial J}{\partial t} = \frac{1}{\mu_0 \sigma(t)} \frac{1}{r} \frac{\partial}{\partial r}\left(r \frac{\partial J}{\partial r}\right) \qquad (1)$$

+) It is created by a separate preionization source.



and polodial magnetic field relaxation

$$L' \frac{dI_p}{dt} + I_p R'(t) = E_T(t) \qquad (2)$$

must be solved simultaneously for the function $\sigma(t)$ under consideration. From Maxwell's equations the field diffusion equation is obtained if the displacement current is neglected and plasma field E and current density J are assumed to have axial (toroidal) components only. The coefficient on the right hand side of Eq.(1) is an effective diffusion coefficient, from which a typical time of radial field penetration is obtained:

$$\tau_{diff} \propto \frac{a^2}{2 D_{eff}} = \frac{1}{2} a^2 \mu_0 \sigma(t) \qquad (3)$$

The relaxation equation (2) relates the total plasma current $I_p = \int 2\pi r J \, dr$ and the impressed field strength $E_T$ with the specific inductance L' and the ohmic resistance $R'(t) = (a^2 \pi \sigma(t))^{-1}$. L' is assumed to be independent of time+). The corresponding relaxation time is written

$$\tau_{L/R} = a^2 \pi \sigma(t) L' \qquad (4)$$

Note that the functions $\tau_{diff}$ and $\tau_{L/R}$ are nearly identical.
a = plasma-(limiter-)radius.
Let us estimate the importance of the skin effect. The diffusion time $\tau_{diff}$ is the time which is necessary for a perturbation in current density at the boundary r = a to

+) The inductance is given by

$$L' = \frac{\mu_0}{2\pi}\left\{ \ln \frac{b}{a} + \frac{\int B_{pol}^2 r' dr'}{a^2 B_{pol}^2(a)} \right\}$$

b = radius for $B_{pol}=0$ (approx. radius of copper shell). During the avalanche phase the current distribution can be assumed homogeneous and the second term in parenthesis becomes 1/4. So we obtain $L' \simeq 2 \cdot 10^{-9}$ H/cm.

propagate to the axis. As long as $\tau_{diff} \ll J/\frac{\partial J}{\partial t}|_{r=a}$ the field penetration is fast enough and J is constant across the radius. For $\tau_{diff} \simeq J/\frac{\partial J}{\partial t}|_{r=a}$ the current density at the axis is retarded $J(t-\tau_{diff})$ in comparison with the boundary J(t).

As a consequence J(a) > J(o), i.e. current density and plasma field too have hollow profiles which is typical for the skin effect. A similar result can be obtained from the following argument. We solve Eq.(1) with the assumption $\partial J/\partial t = \gamma J$. The solution which is finite at the axis is the modified Besselfunction. Therefore we obtain $J(a)/J(0) = I_0(\sqrt{\mu_0 \sigma \gamma}\, a)$ and for $\gamma = \tau_{diff}^{-1}$ $J(a)/J(0) \simeq I_0(\sqrt{2}) \simeq 1{,}6$. For an estimation we substitute $J/\frac{\partial J}{\partial t}|_a \simeq I_p/\frac{dI_p}{dt}$ and neglect the skin-effect whenever the condition

$$\tau_{diff} \leq I_p/\frac{dI_p}{dt} \qquad (5)$$

is fulfilled.

The plasma current $I_p$ we get from a solution of Eq.(2) after specification of $\sigma(t)$ and $E_T(t)$. For the initial condition $I_p(t=0)=0$ the solution can be written as

$$I_p(t) = \exp-\Big[\int_0^t \frac{dt'}{\tau(t')_{4\pi}}\Big] \cdot \int_0^t \frac{E_T(t'')}{L'} \exp\Big[\int_0^{t''} \frac{dt'}{\tau(t')_{4\pi}}\Big] dt'' \,. \qquad (6)$$

The question arises what special function should be used for $\sigma(t)$. In the following parts 3.2 and 3.3 it is shown that at the beginning of the avalanche phase $\sigma(t)$ varies nearly exponentially. At the end of the process the plasma is fully ionized and its conductivity $\sigma_\infty$ is independent on the density. A simple formula which reproduces these facts is

$$\sigma(t) = \frac{\sigma_0 \sigma_\infty e^{\gamma_1 t}}{\sigma_\infty + \sigma_0 e^{\gamma_1 t}} \qquad (7)$$

where $\sigma_0$ corresponds to the conductivity at the start time. We have evaluated the plasma current $I_p(t)$ for a jump of the field $E_T$ = 0.2 V/cm at t = o; $\sigma_0 = 10^{-2}(\Omega m)^{-1}$



and $\sigma_\infty = 5 \cdot 10^2\ (\Omega m)^{-1}$, and $\gamma_1 = 3 \cdot 10^4 s^{-1}$. The initial value of the conductivity corresponds to a density of the preionized plasma of $n = 10^8 cm^{-3}$, and $\sigma_\infty$ to a fully ionized 10 eV plasma. The other parameters are $R_T$ = 40 cm, a = 7.5 cm and L' = $2 \cdot 10^{-9}$ H/cm.

In Fig. 6a the result of the numerical calculation is plotted together with the value $I_p(t)$ for L' → 0. At the very beginning (t < 20 µs) the plasma current shows a delay in comparison with the curve for L' → 0, another delay is obtained before the current reaches its stationary value. At medium times the current grows with the same rate as the conductivity.

In the Fig. 6a the ohmic component of the plasma field is also shown. In Fig. 6b the relation $\tau_{diff}/(I_p/\frac{dI_p}{dt})$ has been plotted. As is clearly seen, only during the time interval 320...460 µs the skin effect is expected to be significant. During the major part of the avalanche phase it can be neglected, and in the early state up to t ≲ 300 µs the growth rate of the conductivity can be obtained from the plasma current.

3.2 Plasma resistance and mean electron density

The electron density in the avalanche phase is less than $n = 10^{12}\ cm^{-3}$. We have no possibility to measure it directly since the 4 mm µ wave interferometer does not operate at these low densities. Therefore we estimate the electron density evolution from the Ohmic part of the plasma resistance with the assumption that Eq.(5) is fulfilled. Using Eq.(2) we get

$$\frac{E_T(t) - L' \frac{dI_p}{dt}}{I_p} = R'(t) \simeq \left(a^2 \pi \sigma(t)\right)^{-1} \qquad (8)$$

σ(t) can easily be obtained from the measured loop voltage and current.

Electron neutral collisions as well as Coulomb collisions determine the plasma conductivity. Using the drift velocity in hydrogen at high values of E/p (cf. Sec. 3.3) and

accounting for the decreasing number of H-atoms the electron neutral collision dominated conductivity is obtained to:

$$\sigma_{eo} = 1{,}8\cdot 10^{-4}\,\frac{n}{(n_H - n)\sqrt{E/n_H}} \qquad cm^{-3}, V/cm, (\Omega cm)^{-1} \quad (9)$$

$n_H$ is the initial density of hydrogen atoms. The Coulomb term of the conductivity is given by

$$\sigma_{ei} = 1{,}9\cdot 10^{2}\,\frac{T_e^{3/2}}{Z\,ln[K T_e^{3/2} Z^{-1} n^{-1/2}]} \qquad (10)$$

with $K = 3{,}9\cdot 10^{9}$ ($T_e \ll Z^2 \cdot 13{,}6$ eV) or $1{,}55\cdot 10^{10}$ ($T_e \gg Z^2 \cdot 13{,}6$ eV). The total conductivity follows from

$$\sigma^{-1} = \sigma_{eo}^{-1} + \sigma_{ei}^{-1} \qquad (11)$$

Eqs.(8) to (11) can be used to determine the mean electron density from the experimental value of the ohmic plasma resistance or conductivity.

3.3 The time constant of electron density evolution

3.3.1 Ionization process

The electron density grows exponentially during the first 200...300 µs. There is a balance between ionization rate $\gamma^i$ and carrier losses $\beta$. For $\gamma^i > \beta$ an exponential growth is predicted:

$$n \propto e^{(\gamma^i - \beta)t} \qquad (12)$$

The ionization frequency $\gamma^i = \alpha(E)\, v_d(E)$ is given by Townsends first coefficient $\alpha$ and the drift velocity $v_d$. Both quantities are functions of the plasma electric field. For sufficient low values of E/p the electrical force eE is balanced by the frictional force of electron neutral collisions $m n_H v_d^2 q_{eo}(v_d)$ resulting in a constant drift velocity. $q_{eo}$ ist the momentum transfer cross section. For hydrogen molecules $q_{eo} \simeq 1{,}8\cdot 10^{-15}$ cm$^2$ is constant at low values of the mean electron velocity



$v_d$ and decreases like $v_d^{-4}$ at high values of $v_d$. So we assume $q_{eo}(v_d) = 1{,}8\cdot 10^{-15}\; v_d^4/(v_o^2 + v_d^2)^2$ with $v_o = 2{,}5\cdot 10^{-8}$ cm/s taken from MÜLLER /11/. The calculated drift velocity $v_d$ vs E/p is plotted in Fig. 7 together with the measurements of SCHLUMBOHM /12/. The experimental points are well approximated in the region $1{,}5\cdot 10^2 < E/p < 6\cdot 10^2$ by the lower branch of the theoretical curve. For stronger values of E/p the distribution function becomes strong non maxwellian. A recent paper of KUSNETSOV and LEBED /15/ solved this problem for high temperature plasmas. Usually, for $E/p > 6\cdot 10^2$ the theory predicts run away electrons, the experiments of SCHLUMBOHM however show that up to $E/p \simeq 2\cdot 10^3$ the drift model seems to be still valid. Therefore the approximation

$$v_d = 6\cdot 10^6\,(E/p)^{1/2} \qquad (cm/s, V/cm, Torr) \quad (13)$$

can be used within the range of $10^2 \lesssim E/p \lesssim 2\cdot 10^3$. PAPOULAR /4/ assumed for the drift velocity $\sim 3{,}5\cdot 10^5\, E/p$ extrapolated from measurements at small E/p.

Similar discrepancies exist for the first TOWNSEND coefficient, too. The values for $\alpha/p$ given by various authors are plotted in Fig. 8. At high values of E/p a significant part of the electrons is in the run away state and does not contribute to ionization. This is a consequence of the ionization cross section which drops considerably with increasing parallel energy. Measurements of BUFFA et.al. /16/ are in accordance with this idea. The effect has been stdied in detail in the theoretical paper of MÜLLER /11/. In Fig. 8 taken from MÜLLER only the upper and lower limits of $\alpha/p$ are shown since the effect is sensitive to several parameters.

3.3.2 Drift losses

The loss processes are strongly related to the spiral particle trajectories inside the torus caused by the centrifugal and the toroidal drift as well as the helical motion due to the external magnetic fields $B_v$ and $B_h$. Electrons starting from the center of the vacuum chamber attain the limiter

radius after a finite life time $t_1$ and are lost. Diffusive losses are negligible comparing with this process. We refer to an analysis of the different electron drift orbits in tokamak geometry given by KNOEPFEL and SPONG /13/ to calculate the drift losses. Fig. 9 shows the situation for the TM 1 in the usual notation. Plasma current and toroidal magnetic field $B_T$ are parallel and the electron drift velocity $v_d$ is antiparallel to $B_T$. The poloidal field $B_{pol}$ is clockwise. The external fields $B_h$ and $B_v$ generated by separate windings have the directions indicated in Fig. 9. The electron guiding center velocity may be broken up into the following components:

The centrifugal drift velocity $\frac{v_d^2}{\frac{e}{m}|B_T|R_T}\frac{\vec{R}_T\times\vec{B}_T}{|\vec{R}_T|\,|\vec{B}_T|}$ and the toroidal drift $\frac{1}{2}v_\perp\rho_c\frac{\vec{B}\times\nabla|\vec{B}|}{|\vec{B}|^2}$ which are in the -z direction ($v_{z2}$). A third component is due to $B_v$. The resulting toroidal field is slightly downward directed, and the electron drift velocity gets an upward directed component $v_{z1}$. So we have

$$v_z = -\left(\frac{e}{m}B_T R\right)^{-1}\left(v_d^2+\tfrac{1}{2}v_\perp^2\right) + v_d\frac{B_v}{B_T} = v_d\frac{B_v-B_1}{B_T} \qquad (14)$$

where an equivalent vertical field

$$B_1 = \left(v_d+\tfrac{1}{2}v_\perp^2/v_d\right)\left(\frac{e}{m}R\right)^{-1} \qquad (15)$$

is introduced, which accounts for the centrifugal- and toroidal drift. Similar to $v_{z1}$, the horizontal field gives an x-component of the drift velocity:

$$v_x = -v_d\cdot B_h/B_T\ . \qquad (16)$$

The poloidal magnetic field causes a helical motion of the guiding center. The magnetic field is clock wise, therefore the electron velocity is anti-clockwise

$$v_{pol} = v_d\cdot B_{pol}(r)/B_T = \omega r \qquad (17)$$



The resulting velocity is the vector sum of Eq.(14) to (17):

$$v_z = v_d\frac{B_v-B_1}{B_T} + \omega x \qquad (18)$$

$$v_x = -v_d\frac{B_h}{B_T} - \omega z \qquad (19)$$

From these equations it follows, that the projection of the individual particle trajectories to the x-z- plane are coaxial circles in a general position with

$$x_c = -\frac{v_d}{\omega}\cdot\frac{B_v-B_1}{B_T} \qquad (20)$$

and

$$z_c = -\frac{v_d}{\omega}\frac{B_h}{B_T} \qquad (21)$$

as the centre coordinates, Fig. 10. The particles move anticlockwise in $\omega$-direction. For an electron with the coordinates $P_o(x_o,z_o)$ at $t = 0$ the radius of the trajectory circle $R_t$ follows from the equation

$$R_t = \sqrt{(x_o-x_c)^2+(z_o-z_c)^2} \qquad (22)$$

These results are only correct for a homogeneous current density distribution, i.e. if the poloidal velocity is a linear function of r acc. to Eq(17). An electron moving from $P_o$ to $P_1$ has the drift time $t_d$, which can be calculated from the x-component of the velocity $v_x = dx/dt$ acc. to (19). After integration we obtain

$$\omega t = \arcsin\frac{x_o+|x_c|}{\sqrt{1+m^2}\,|x_o+|x_c||} - \arcsin\frac{x_1+|x_c|}{\sqrt{1+m^2}\,|x_o+|x_c||}$$

$$x_1 = \frac{F\pm m\sqrt{(1+m^2)a^2-F^2}}{1+m^2}\ ;\quad F = \frac{R_t^2-|x_c|^2-|z_c|^2-a^2}{2\,|x_c|} \qquad (23)$$

$$m = \frac{|z_c|}{|x_c|} = \frac{B_h}{B_v-B_1}\ ;\quad \omega = \frac{v_d B_{pol}(r)}{r\,B_T} = \frac{26{,}7\,v_d\,I_p}{a\cdot B_T}$$

$(s^{-1}, cm, kA, G)$

From these equations it follows, that for any given start position $x_o, z_o$ the drift time $t_d$ only depends on the parallel drift velocity $v_d$ and the different magnetic fields. Note that $B_{pol}$ is a function of $I_p$.

Two main regions of drift losses can be distinguished from geometrical considerations of Fig. 10:

a) the center of the trajectory circle is outside the limiter radius a, and

b) the center is inside.

The transition is given by the condition $\sqrt{x_c^2 + z_c^2} = a$ or

$$\sqrt{(B_v - B_1)^2 + B_h^2} = 26{,}7 \cdot I_p \quad (B, kA) \qquad (24)$$

In case a) all particles drift to the limiter radius, no particles are confined. For a sufficient strong plasma current a well defined number of particle trajectories are closed lines and remain inside the limiter radius (case b), that means the electrons have infinite life times.

Since the plasma current is very small during the start phase we are in region a). For different values of the magnetic fields $B_v, B_h$ and plasma currents from 0,1 kA (experimental limit) up to the value given by Eq(24) $t_d$ is calculated as a function of $x_o$. Fig. 11 shows examples for two sets of magnetic fields. All particles are assumed to start from the straight line A-C (Fig.10) with different values of $x_o$. For sufficient low plasma currents, electrons which start from the centre ($x_o = z_o = 0$) have maximum drift times $t_1$. The curves have more asymmetric shapes with increasing plasma current. In general, however, in region a) the influence of $I_p$ is not very significant. For small currents compared with Eq(24) the maximum drift time is approximately given by

$$t_1 \simeq \frac{a B_T}{v_d \sqrt{(B_v - B_1)^2 + B_h^2}} \qquad (25)$$

independent from $I_p$. This formula predicts a clear dependence of $t_1$ on the external magnetic fields, which should



be observable in the experiment.

## 4. Comparison with the experiment

### 4.1 Plasma resistance and mean electron density

Fig. 3 shows a logarithmic plot of the plasma current for three typical shots with different values of the external perpendicular field $B_\perp$. Two shots show an exponential increase at the beginning with $\gamma$ between 3 and $5 \cdot 10^4\ s^{-1}$, the remaining one is more complicated.

If we disregard the periodic structure of this curve, we obtain $\gamma \simeq 10^4\ s^{-1}$. From these curves and the associated values of the loop voltage the ohmic plasma resistance $Z_{\Omega}$ is calculated (Fig. 12). After an exponential decrease during the avalanche state the plasma resistance attains a minimum value of about $3 \cdot 10^{-3}$ Ohms which corresponds to a conductivity of $5 \cdot 10^2\ \Omega^{-1} m^{-1}$, well identified as the Coulomb conductivity of a fully ionized 10 eV plasma. The electron density during the avalanche state is calculated from Eq's (8) to (11) assuming $n_H = 10^{13}\ cm^{-3}$, $Z = 1$, $T_e = 10$ eV and the actual value of E, which is between 0,12 and 0,36 V/cm, see Fig. 13. The values of $\gamma$ and $n(t=0)$ are given in the table.

| Current of external field coils | $I_h$ | 100 A | 175 | 300 |
|---|---|---|---|---|
| | $I_v$ | 200 A | 600 | 800 |
| $\gamma$ | | $4 \cdot 10^4\ s^{-1}$ | $3{,}3 \cdot 10^4$ | $10^4$ |
| $n(t=0)$ | | $5 \cdot 10^8 cm^{-3}$ | $3 \cdot 10^8$ | $6 \cdot 10^9$ |

### 4.2 The transverse field components

The transverse field components $B_v, B_h$ in Eq.(25) are the actual magnetic fields within the plasma. They are combinations of several components, only some of them can be calculated or measured doubtless /14/:

1. The deliberately applied fields $B_v^{ext}$ and $B_h^{ext}$ generated by external currents parallel to the plasma axis which control the plasma position.

2. Perpendicular fields caused by the inhomogeneous distribution of the current in the liner and by eddy currents in the copper shell.

3. $B_\perp$-components from the misalignment of the toroidal field coils.

4. Stray fields from the iron transformer core.

The contributions 2,3,4 can hardly be calculated but they play a role at the beginning of the start up phase when the liner current is bigger than the plasma current. We tried to measure these fields by means of the MIRNOV coils. The result was $B_v^{int} = -8{,}4 \cdot 10^{-4}$T, $B_h^{int} = -11{,}4 \cdot 10^{-4}$T in opposite direction to the external fields acc. to 1.

The procedure was as follows:
The starting position of the plasma is sensitive to the perpendicular fields $B_v$ and $B_h$. Acc. to Sect. 3.2 the plasma starts at those positions near the liner the trajectories of which predict a maximum drift time. At this period the MIRNOV coil signals are too weak and give no information. The centre of all particle circles moves toward the axis of the liner along a straight line A-C when the plasma current increases, compare Fig. 10. The inclination angle $\varphi$ of this line can now be measured from the ratio of the time integrated difference signals of the vertical and horizontal pairs of MIRNOV coils. A series of measurements with different values of $B_v^{ext}$ and $B_h^{ext}$ gives the above values of the internal fields. Mainly two facts, however, limit the accuracy of this method:

a) The internal fields are determined at the position of the MIRNOV coils, it is doubtful wether they are constant along the circumference of the torus.



b) The measurements are possible only at times with sufficient strong plasma current ( $>300/\mu s$) when the avalanche state has just finished.

Therefore it is necessary to look for some additional hints for the magnitude of the actual perpendicular fields $B_\perp = B_\perp^{ext} + B_\perp^{int}$ during the avalanche phase.
We measured the $B_\perp$-dependence of some quantities which are related to breakdown. In Fig. 14 there are shown: the time of the first maximum of the probe ion saturation current; the first deviation of the loop voltage with plasma breakdown from the trace without breakdown; the first maximum of the probe floating potential; the plasma resistance $Z_{\mathcal{U}}$ at a fixed time $200/\mu s$ in dependence on the $B_v$-field and the jump of the probe first peak from electron to ion current as a function of the $B_v$ and $B_h$ fields. The jump can only be observed if the probe is located at the edge of the limiter projection and connected via 80 Ohm to the liner potential. The effect has not been investigated in detail but is obviously caused by a rapid change of plasma potential.
The minima of all these curves are shifted by $B_v \simeq 3 \cdot 10^{-4}$T and $B_h \simeq 6{,}5 \cdot 10^{-4}$T with respect to the zero $B_\perp$-field. Supposing that the breakdown conditions are optimal for $B_\perp = 0$ we conclude the internal fields to these smaller values. The model shows (Eq.(25)) that there are no particle drift losses in the avalanche phase for vanishing $B_\perp$, i.e. $\gamma$ is maximum. DENISOV et.al. /9/ measured an internal field of $B \simeq 7 \cdot 10^{-4}$T in Tokamak T7, and SOMETANI /7/ $B \simeq 5 \cdot 10^{-4}$T in the JFT 2 installation by a similar procedure.

4.3 Determination of ionisation coefficients $\alpha$ and $\gamma_i$

In order to explain the exponential growth of current and density in the start up phase we discuss the loss processes caused by the $B_\perp$-fields. Fig. 15a shows the inverse time constant for current growth as a function of the actual perpendicular field.

A clear dependence on $B_\perp$ is obtained (correlation coefficient $r \simeq 0{,}6$), whereas the use of the stronger values give results where this dependence ist not significant ($r \simeq 0{,}24$). If we assume, that the decrease of $\gamma_2$ is caused by the drift losses, we can use the quantity $t_1$ acc. to Eq.(25) which represents the particle losses for a substantial central part of the plasma volume.

Substituting $\beta = 1/t$ with $t_1$ from Eq.(25), $v_d \simeq 3 \cdot 10^8$ cm/s, $a = 7.5$ cm $B_T = 1{,}3$ T and $\gamma_2$ from the measurements we obtain the ionisation frequency $\nu^i$ from $\gamma^i = \gamma + \beta$ independent on $B_\perp$ as expected, compare Fig. 15b. In order to calculate the corresponding value of the first TOWNSEND coefficient $\alpha = \nu^i / v_d$ we assume that during the avalanche state the hydrogen molecules are not yet dissociated. Then from the filling pressure of the chamber $\simeq 1{,}3 \cdot 10^{-2}$ Pa and with $v_d = 3 \cdot 10^8$ cm/s $\hat{=}$ E = 0,25 V/cm we get from Fig. 15b $\alpha/p = 2{,}2$ within the expected range of values, Fig. 8.

## 5. Conclusions

The following conclusions can be drawn from this experiment:

1. The time delay between the start of the OH battery and the first signal of plasma current and density is determined by the exponential growth of an electron avalanche starting from the density given by the preionization source.
2. The carrier production is controlled by the electron drift velocity in the toroidal electric field and not by thermal ionisation.
3. After the exponential phase a pinch occurs where the plasma looses the wall contact, the temperature increase up to 20 eV and the ionization becomes thermal. Current density and electron density grow much slower than in the avalanche state. The conductivity is that of a fully ionized plasma.



4. The time constant in the exponential region is given by a balance of ionization and carrier losses. We have shown that the carrier losses are determined by the auxiliary perpendicular magnetic fields which control the different drift motions of the electrons in the avalanche state. The smallest losses, i.e. the fastest current rise occur for vanishing perpendicular fields.
5. These fields are not only given by the externally applied fields, but also by some internal fields caused by different imperfections of the real tokamak geometry. We tried to measure these fields by different methods and get results between $-3 \ldots -8 \cdot 10^{-4}$ T for the vertical and $-6{,}5 \ldots -11{,}4 \cdot 10^{-4}$ T for the horizontal component. These fields cannot be influenced within the normal working regime of the installation.
6. As long as the conditions $\frac{I_p}{\left|\frac{dI_p}{dt}\right|} \gg \tau_{diff}, \tau_{4R}$ are fulfilled neither the skineffect nor the relaxation of poloidal field growth are significant, and some important plasma parameters may be obtained from measurements of loop voltage and plasma current. These parameters are: current density, electron density, ohmic and inductive part of plasma resistance and electric field inside the plasma. The values fit in the results obtained by the usual diagnostics e.g. microwave interferometer measurements in the later state.
7. The value of the first TOWNSEND coefficient $\alpha/p = 2{,}2$ at $E/p \simeq 2 \cdot 10^3$ V/cm. Torr is only one half of the value known from gas discharge physics. It can be explained by a moderate run away regime, but there are no other experimental indications for that state: hard x-ray, influence on probe characteristics or so.

Two of us (H.P. and P.H.) wish to thank the TM 1 team for cooperation during the experiments and operation of the machine.

## 6. References


/1/ D.L. Dimock et al. Nuclear Fusion 13 (1973) 271

/2/ I.H. Hutchinson, J.D. Strachan; Nuclear Fusion 14 (1974) 649

/3/ J.D. Strachan; Nuclear Fusion 16 (1976) 345

/4/ R. Papoular; Nuclear Fusion 16 (1976) 37

/5/ V.A. Abramov et al., Fizika Plasmy 1 (1975) 536

/6/ V.A. Abramov et al., Fizika Plasmy 3 (1977) 512

/7/ T. Sometani, N. Fujisawa; Plasma Physica 20 (1978) 1101

/8/ J.D. Strachan; J. Nucl. Material 63 (1976) 132

/9/ V.F. Denisov et al., Fizika Plasmy 8 (1982) 238

/10/ J. Datlov et al. Proc. IX. EXXFPP Vol. 1, Oxford (1979),539

/11/ K.G. Müller; Z. Physik 169 (1962) 432

/12/ H. Schlumbohm; Z. Physik 182 (1965) 317

/13/ H. Knoepfel, D.A. Spong; Nuclear Fusion 19 (1979) 785

/14/ V.S. Mukhovatov, V.D. Shafranov; Nuclear Fusion 11 (1971) 605

/15/ Yu.K.Kusnetsov, S.A. Lebed; Fizika Plasmy 8 (1982) 1269

/16/ A. Buffa et al., Phys. Rev. A3 (1971) 955




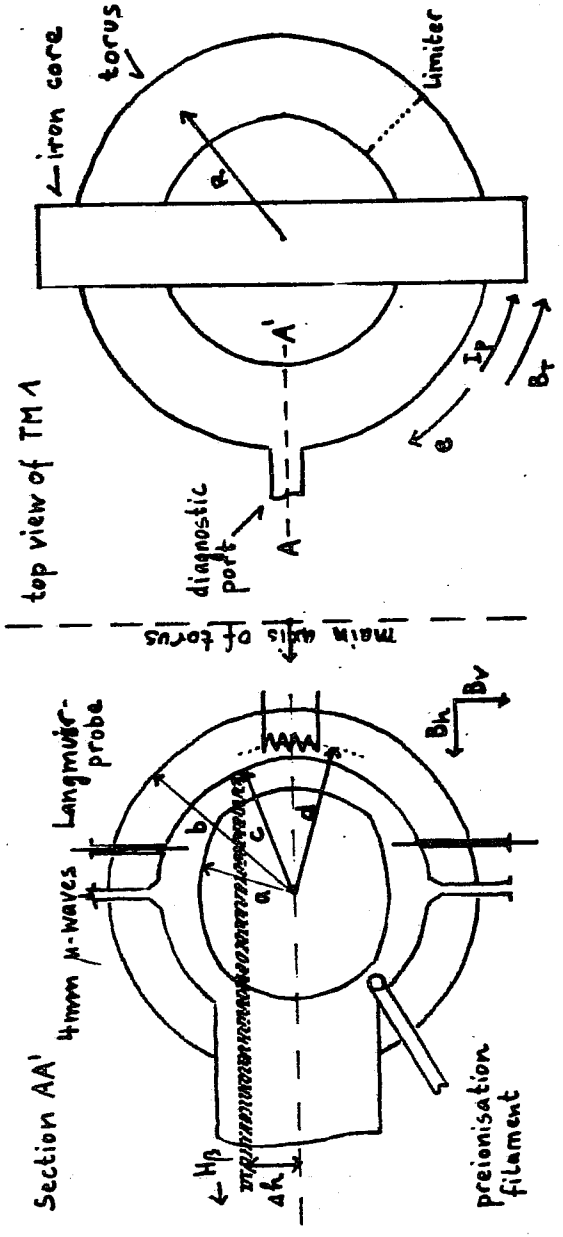


Fig.1
Cross section of the diagnostic part. Limiter and 4 Mirror coils are not located in this section (see top view of TM 1 on the right side). a = 7,5 cm limiter radius; b = 13,5 cm copper shell radius; c = 10,5 cm liner radius; d = 11,5 cm position of Mirror coils

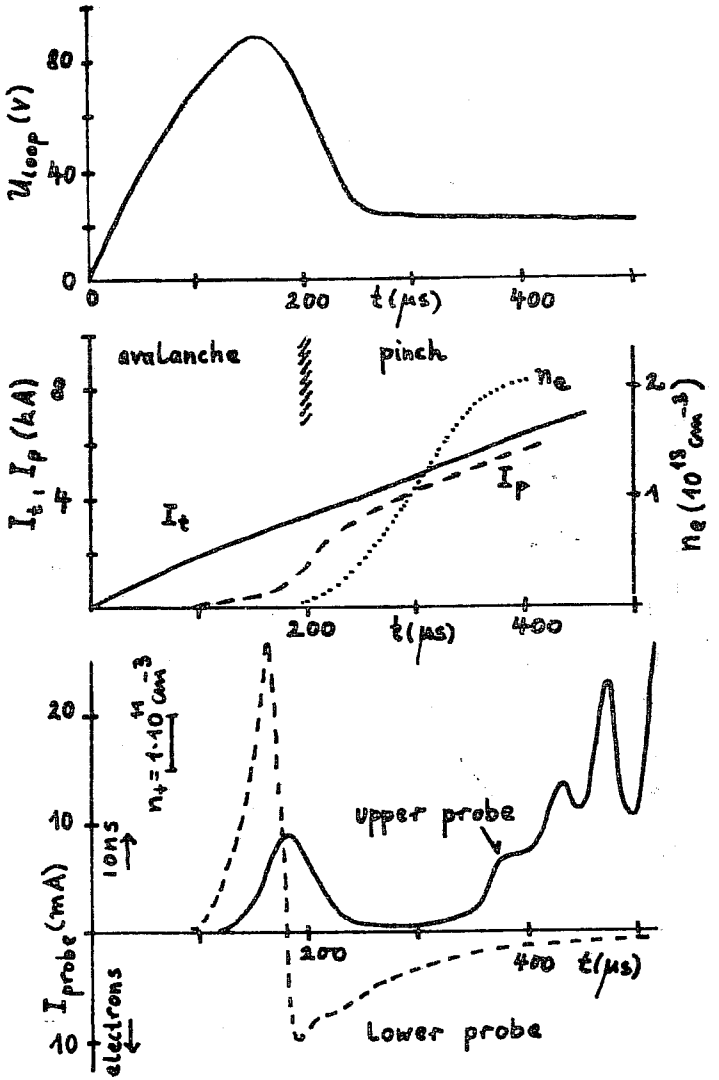


Fig.2
Temporal evolution of the plasma parameter during the first 500 μs after OH-battery ignition. Loop voltage $U_l$; total and plasma current $I_t$, $I_p$; electron density from 4mm μ-waves. The both probes are at r=8cm, $U_p$=-60V.



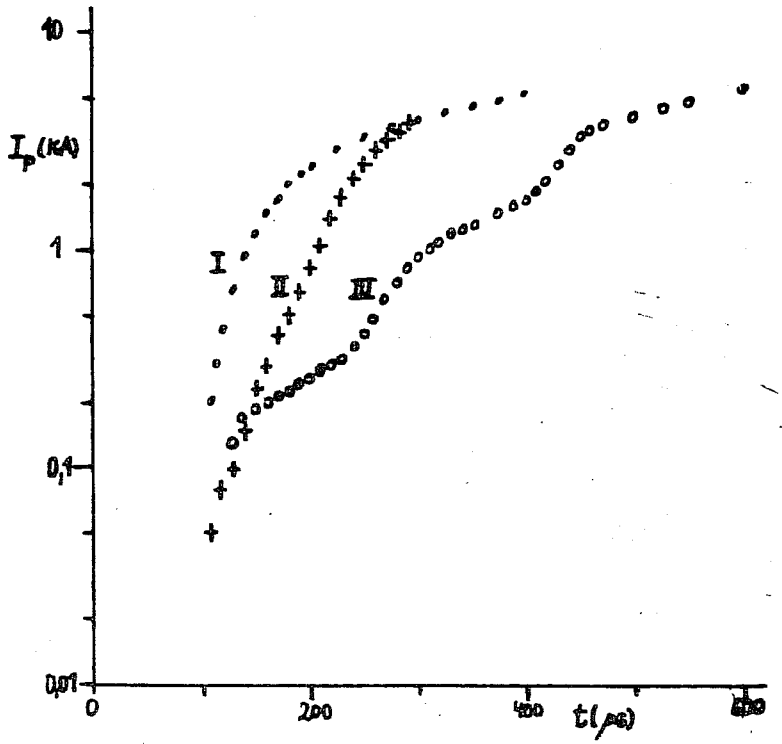


Fig.3
Temporal evolution of the plasma current. CurveI: $B_v$=5,6·$10^{-4}$T, $B_h$=6,5·$10^{-4}$T; Curve II: $B_v$=16,8·$10^{-4}$T $B_h$=11,4.$10^{-4}$T; Curve III: $B_v$=22,4·$10^{-4}$T, $B_h$=19,5.$10^{-4}$T.

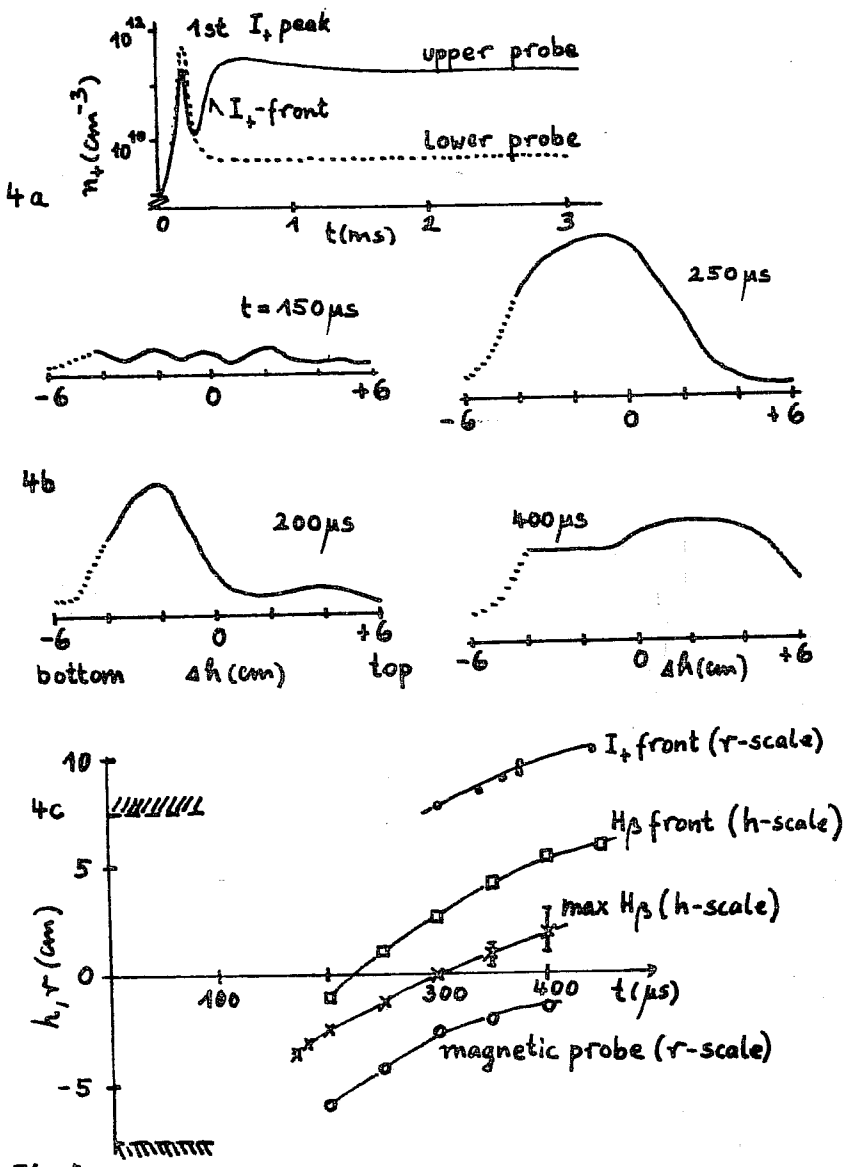


Fig.4
Plasma profile and position during the avalanche phase.
a) Probe signals. b) $H_\beta$-line radiance, c) plasma position.



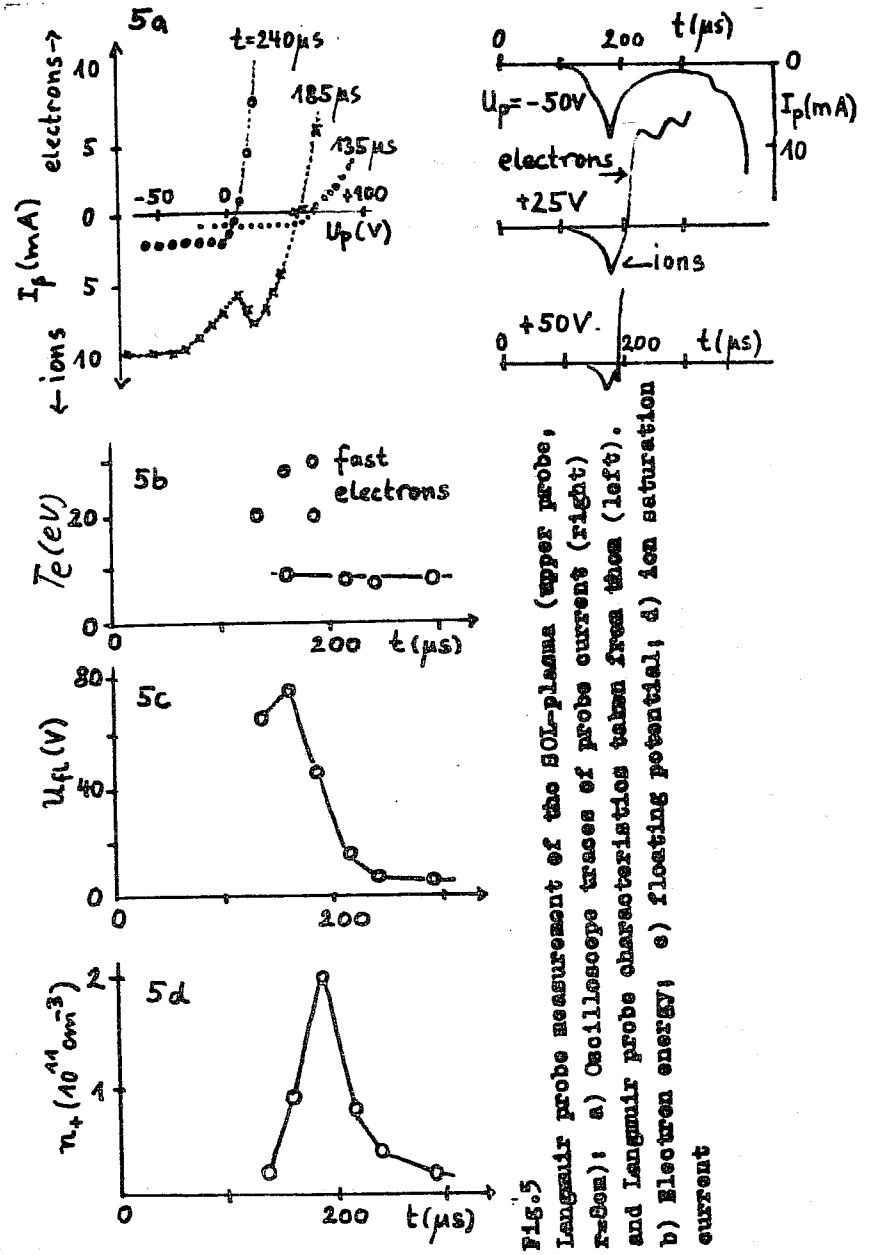


Fig.5
Langmuir probe measurement of the SOL-plasma (upper probe, r=8cm): a) Oscillosoope traces of probe current (right) and Langmuir probe characteristics taken from them (left). b) Electron energy; c) floating potential; d) ion saturation current

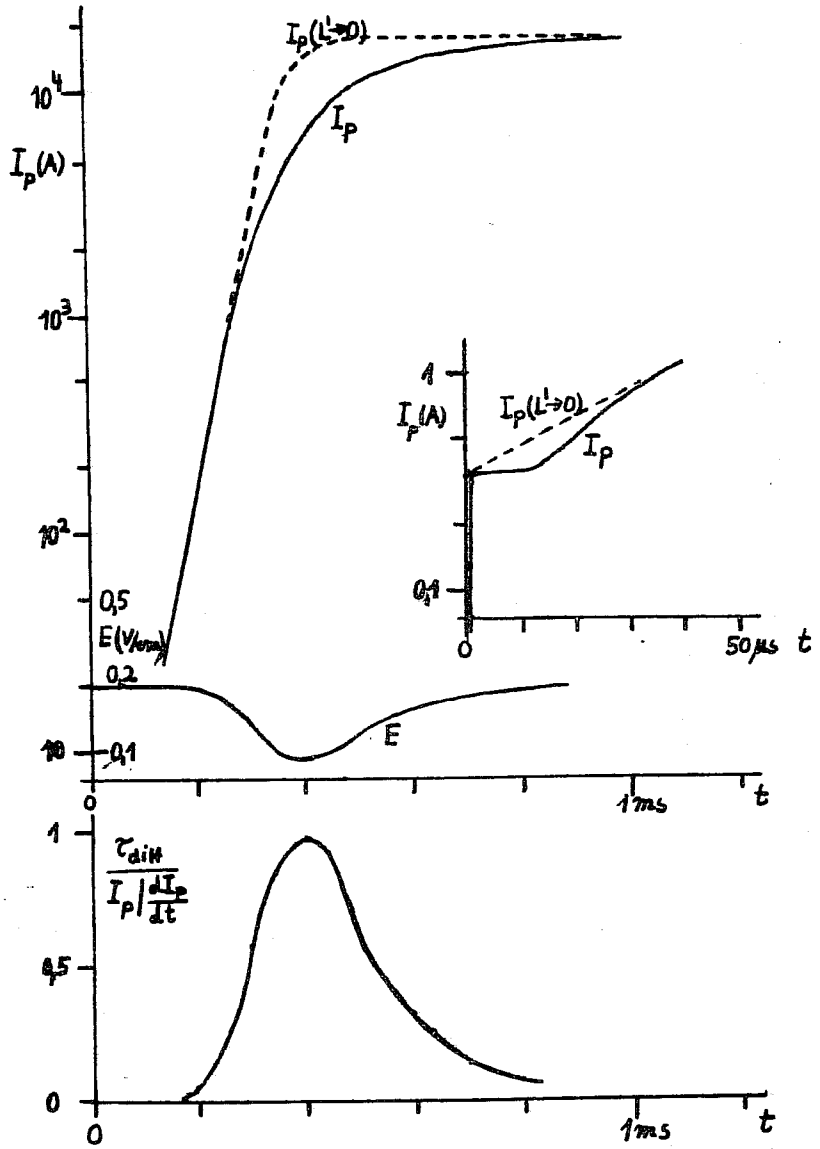


Fig 6a: Temporal evolution of plasma current and field after a jump of the loop voltage at t=o.

Fig.6b: Ratio of field diffusion time to the time scale of plasma current characterizing the skin effect.



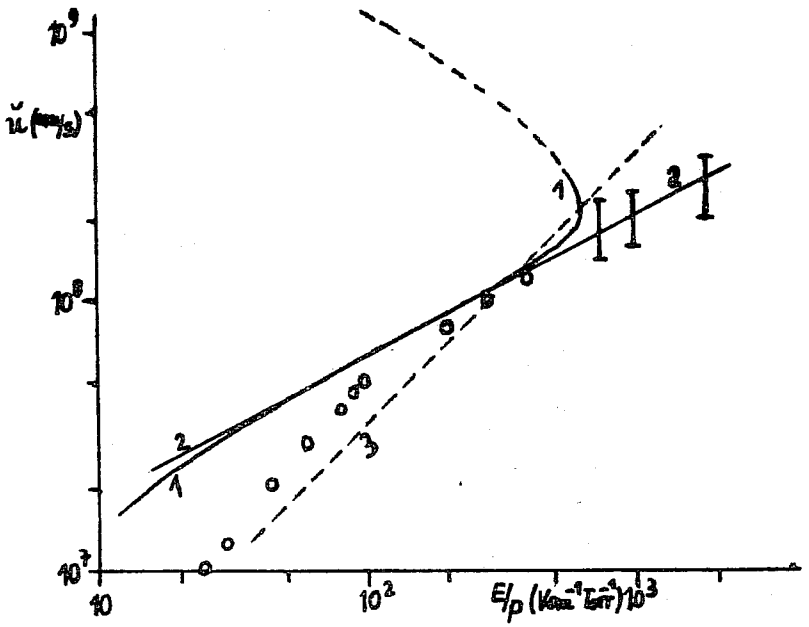


Fig.7
The drift velocity of electrons in molecular hydrogen. ooo, III: experimental values of SCHLUMBOHM /12/. Curve 1: calculated values acc. to MÜLLER /11/. Curve 2: approximation Eq.(13). Curve 3: approximation acc. to PAPOULAR /4/.

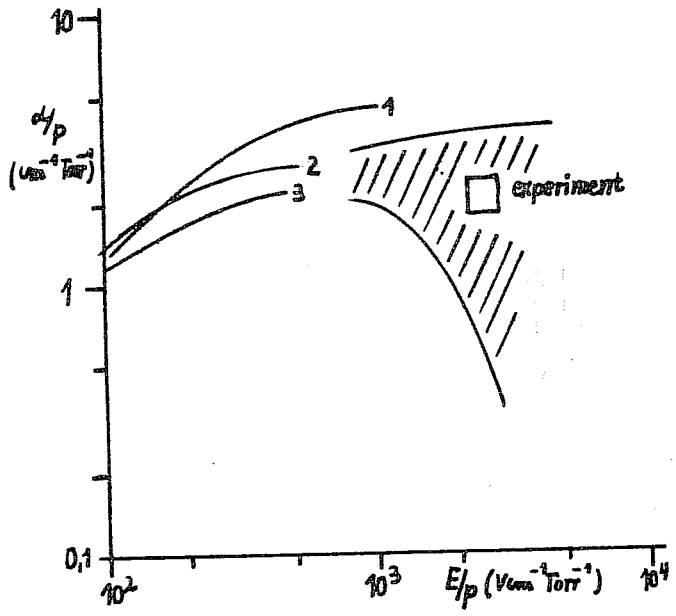


Fig.8
Ionization coefficient in in molekular hydrogen taken from MÜLLER /11/. Curves 1,2,3: classical experimental values from different authors. Hatched area: modification by run away electrons. □: Result of present experiment.



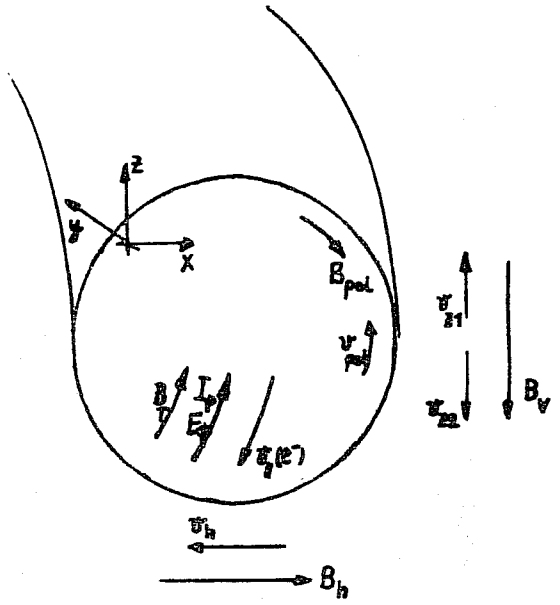


Fig.9
Physical quantities which determine the drift losses.

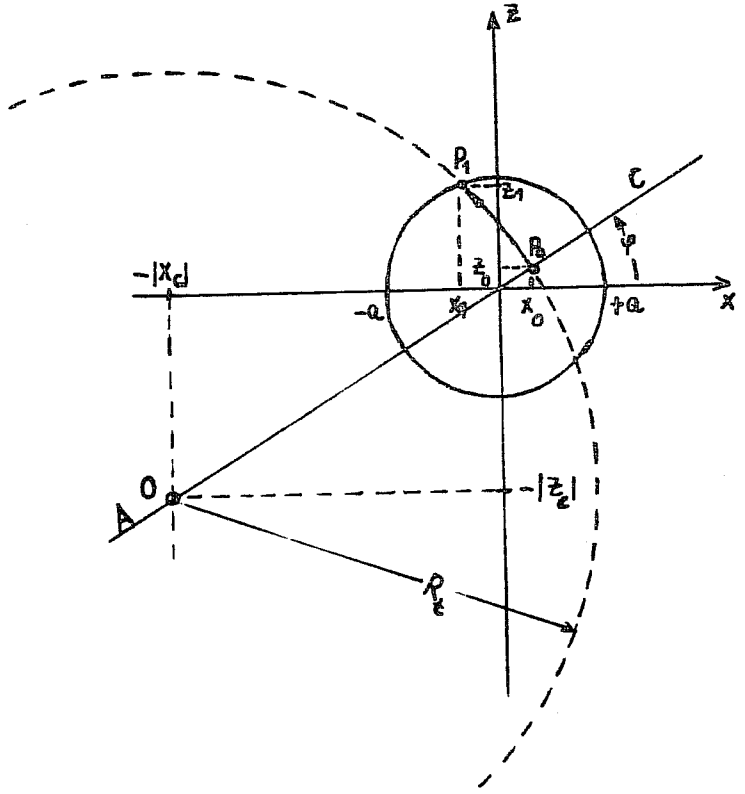


Fig. 10
Drift approximation of particle trajectories.



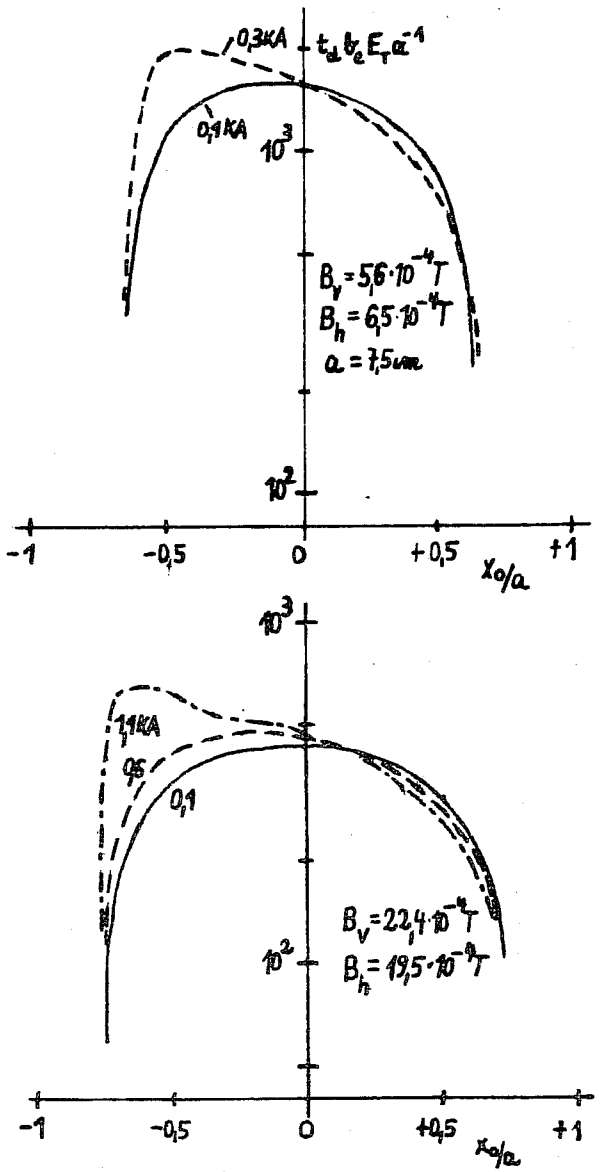


Fig. 11
Normalized drift time $t_d \cdot b_e \cdot E_T/a$ as a function of the start position. $E_T = E_\phi$ is the toroidal plasma electric field.

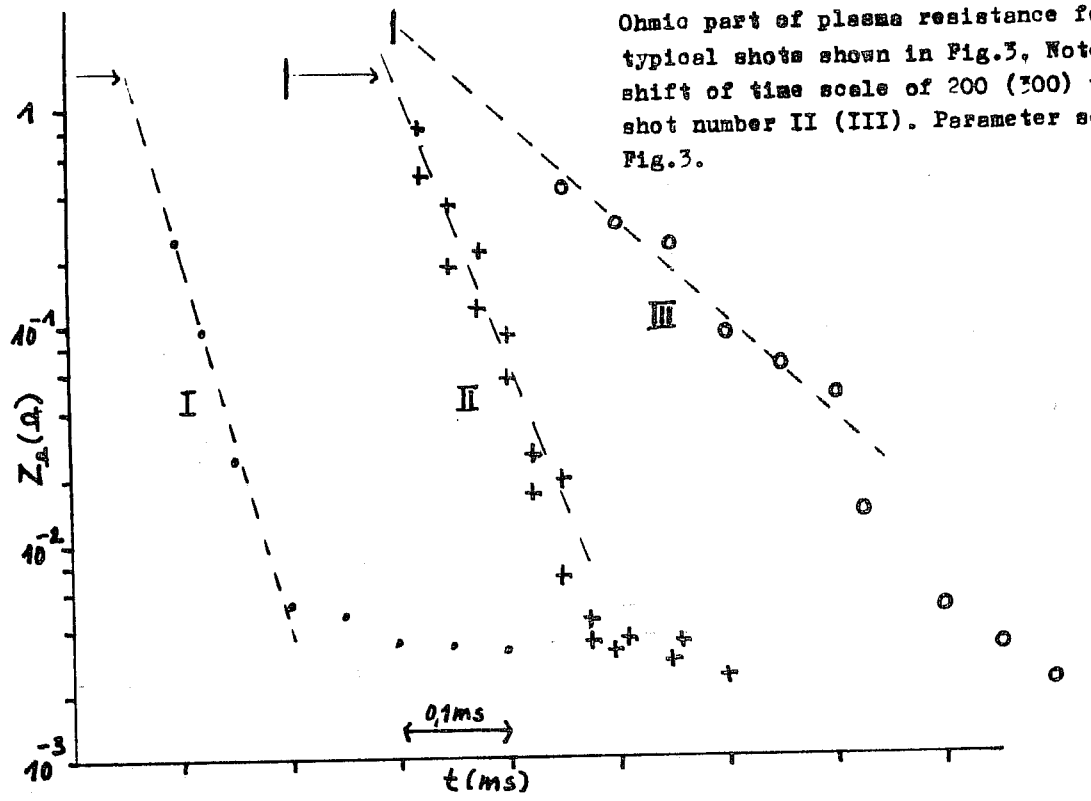


Fig. 12
Ohmic part of plasma resistance for the typical shots shown in Fig.3. Note the shift of time scale of 200 (300) us for shot number II (III). Parameter see Fig.3.

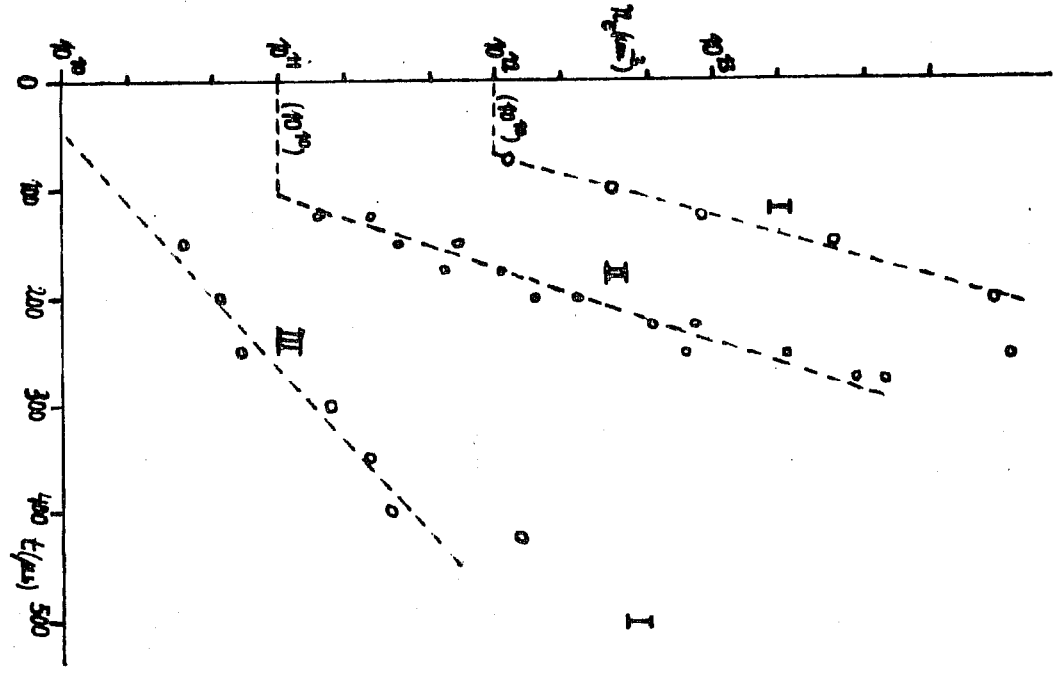


Fig. 13

Temporal evolution of mean electron density for typical shots I-III. The density scale is shifted by 2 (1) orders of magnitude for shot I (II). Parameter see Fig.3.

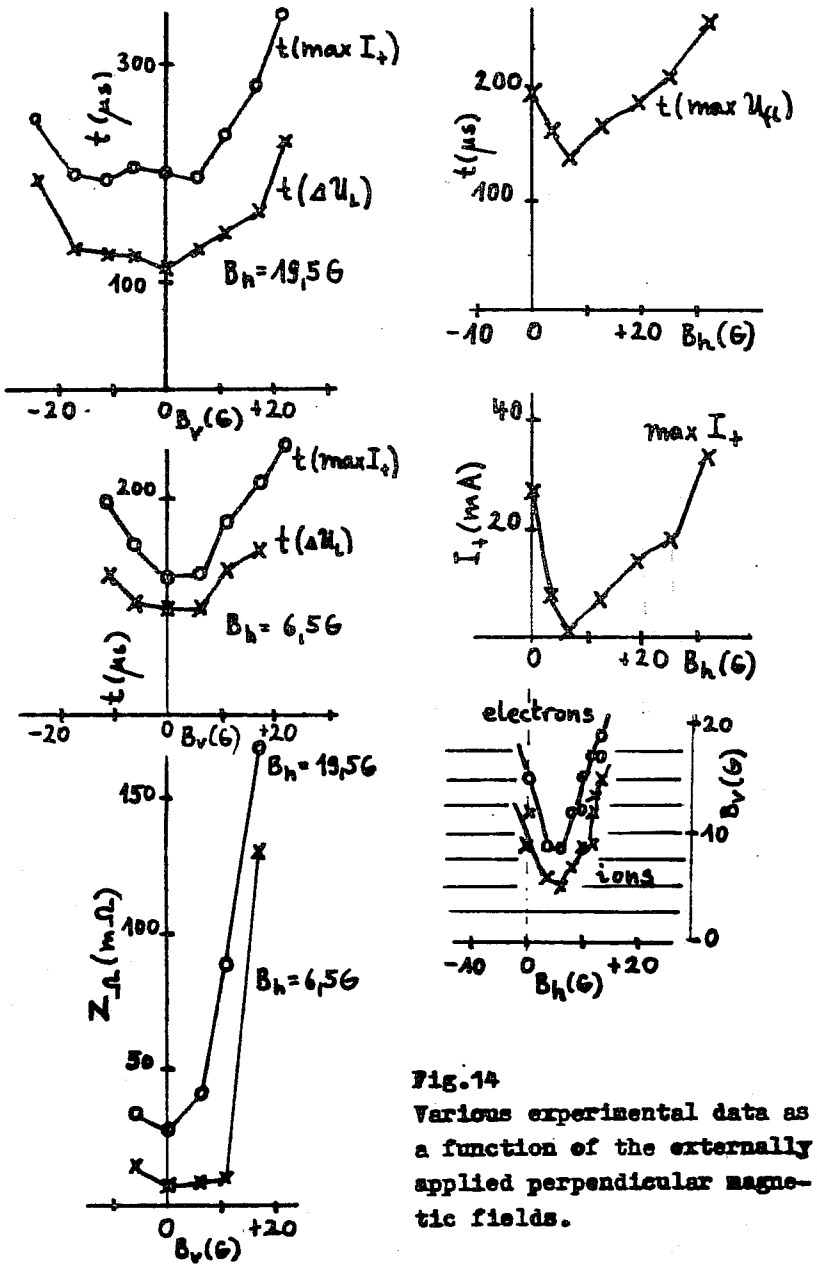


Fig.14
Various experimental data as a function of the externally applied perpendicular magnetic fields.



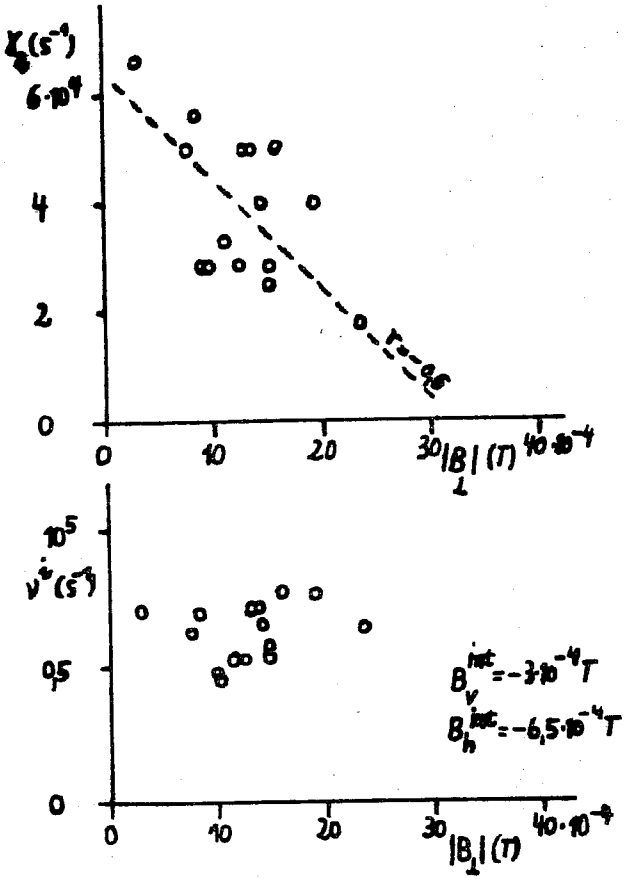


Fig.15
Current growth rate $\gamma_\perp$ and ionization frequency as a function of the total perpendicular magnetic field. The internal fields are taken from the measurements of Fig.14.